Annals Geol. Surv. Egypt, V. XXI. (1998), pp. 535 - 552

A STUDY ON SEA WATER EFFECTS BY USING GEOELECTRIC RESISTIVITY MAPPING AT EL-ADABIYA, GULF OF SUEZ, EGYPT

Mesbah, M. A.

Department of Geological Engineering; Faculty of Pet. and Min. *Eng., Suez*

Suez Canal University' e-mail: mmesbah@frcir.eun.eg

ABSTRACT

Electric resistivity method can be used in mapping zones of contaminated soils and groundwater salinity. A dense electrical resislivity survey was carried out at a site near El-Adabiya harbor (Suez Governorate) in order to assess the impact ofsalt water on geological and hydrogeological environments.

Geologically, the investigated area is composed mainly of alluvial *fans.* ***These fans comprise porous spaces which control the flow of electric current. Therefor-e, the resistivitv of porous media is controlled not only by the amount of solutions, porosity and permeability of the porous media but also by the total dissolved solids in these solutions.***

Horizontal electrical sounding (HES), using Wenner- array, was utilized in order to acquire the apparent resistivity data at different spacings (a). Eight iso-apparent r°esistivity maps were obtained at a's = *1, S, 10, 15, 20, 30, 50 and 60 meters.* ***The contoured iso-apparent resistivity maps were separated, by applying least square polynomial technique into general trends (best fitted regional) and locals (statistically residual). Local maps were resolved into positive and negative zones.***

Low r-esistivity *values* ***(negative zones on the local maps) are attributed to contaminated soils in the uppermost surface layer and to salt water intrusions in the deeper layers. Positive zones are attributed to dry and compact soils in the soil layers and to hard rocks at lower levels.***

INTRODUCTION

Electrical resistivity measurements have been used significantly in groundwater prospecting (e.g. Flathe 1954; Keller and Frischknecht 1966; Zohdy et al. 1974; Telford et al. 1990 and Burger 1992). Since, the resistivity values are controlled mainly by water content, grain size, porosity, fractures, permeability and by the concentration of dissolved solids. Therefore, the electrical resistivity method of prospecting provides detailed information about the geometry, source and amount of contamination (e.g. Bhattacharya et al. 1974; Kelly 1976; Mazac et al. 1987 and Benson 1992). Both the apparent (raw) resistivity values (Topfer, 1976; El-Hefnawy et al. 1984 and AbdelFattah et. al. 1988) and the inverted resistivity values (Lanz et al. 1994; Shendi 1995 and Benson et al. 1997) can be used for such purposes.

The investigated area lies along the base of Gabal Ataqa on the Gulf of Suez coastal zone at El-Adabiya harbor. The northern part of the Gulf of Suez region,

including the study area, has a particular importance from the economic point of view, based on the current national plan for developing this region.

In this work, eight iso-apparent resistivity maps were constructed through apparent resistivity values measured at spacings (a) equal l, 5, 10, 15, 20, 30, 50 and 60 meters, in order to reveal the geoelectric style of the successive layers penetrated by the electric current. It is well known that, the depth of penetration increases according to the comparable increase of the electrode spacing. Apparao and Roy (1971) and Apparo (1991), reported that the maximum depth of penetration in the case of Wenner array equals 0.11 **the distance between the two current electrodes. Therefore, the collected resistivity mapping data will reflect the geoelectric regime at expected depths of 0.33, 1.65, 3.3, 4.95, 6.6, 9.9, 16.5 and 19.8 m. respectively.**

GEOLOGY AND GEOMORPHOLOGY

Geologically, the studied area can be put in its regional situation by drawing the stratigraphic succession of the Gulf of Suez region given by Said (1962). The uppermost part of this succession can be given here as follows:

Pleistocene **Gravel terraces, coral reefs and raised beaches.**

Pliocene **Gravels, interbedded marls and gypsum.** *Miocene* **Lithothamnion limestone. Evaporite series.**

Globigerina marls.

The main geomorphologic features of the Suez area (Fig. 1) were studied in details by Bush et al. (1980). **They can be summarized as follows:**

. - The limestone plateau of Gabal Ataqa with its steep east-facing mountain front.

- The zone of alluvial fans marginal to Gabal Ataqa.

- The coastal fringe of emerged marine features.

The study area is a part of the zone of alluvial fans. It is covered mainly by alluvial and marine deposits. Numerous shallow boreholes were drilled adjacent to the studied area, for construction purposes (Ardaman and Associates 1992). Fig.(2) represents a lithologic description for one of them.

The fans were formed from the debris discharged through numerous drainage basins in Gabal Ataqa. The debris accumulated along the eastern fault-controlled margins of the mass to produce a complex series of segmented alluvial fans. These fans are found as three major types:

(i) Higher Fan Terraces:

These morphological units are found in the embayment between the mountain foot and the outlining fault bounded block. These small surfaces are underlain by deposits of bedded silts, angular and sub-rounded gravels and boulders, up to 15 m in thickness, and represent fragments of the earliest surviving alluvial fan deposits in the area.

(ii) The Older Fans:

These comprise a set of combined and individual fans occupying a zone from 600 to 400 m wide along the base of Gabal Ataqa, with a slope that varies from 1 ° to 10 °. These fans consist mainly of gravels, boulders and silts with little amounts of sands. They have been dissected by a series of wadies that feed the younger fans. The older

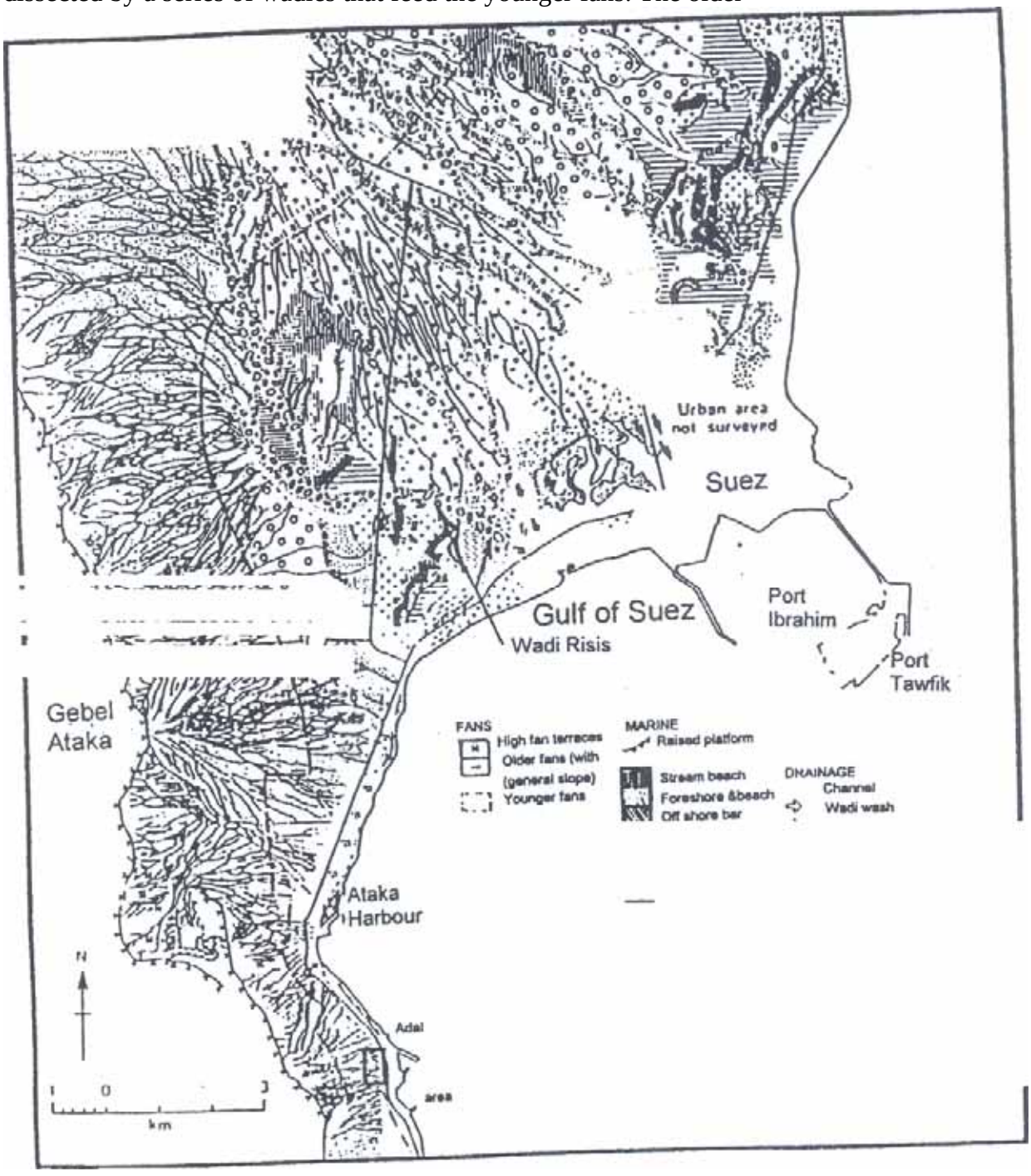

Fig. 1: Geologic - Geomorphologic Map Of Suez Area (After Bush Et AL 1980) 0 The Studied Area

fans disappear eastwards under the younger ones.

(iii) The Younger Fans:

These have developed by entrenchment into the older fans, with a slope range from 0.5° to 2°. So, they are deeply entrenched at the mountain fronts.

In general, it seems that the younger fans have extended eastwards as the sea level has fallen from its higher level, extending toward the exposed marine surface.

The younger fans comprise gravels and boulders with little sands in a silty matrix. Dolomite and limestone clasts are preponderant. They show none of the features

Borehole No.: BHZ **Date: 14/10/1991.**

Ground level: + f3.06 MSI. **Water Depth: NO G.W.L.**

Description

IAL DEPOSITS: Calcareous sandy gravel wtth scme schbles.bcutder: and sflt.ltght brown.
End of boring at 7.Om

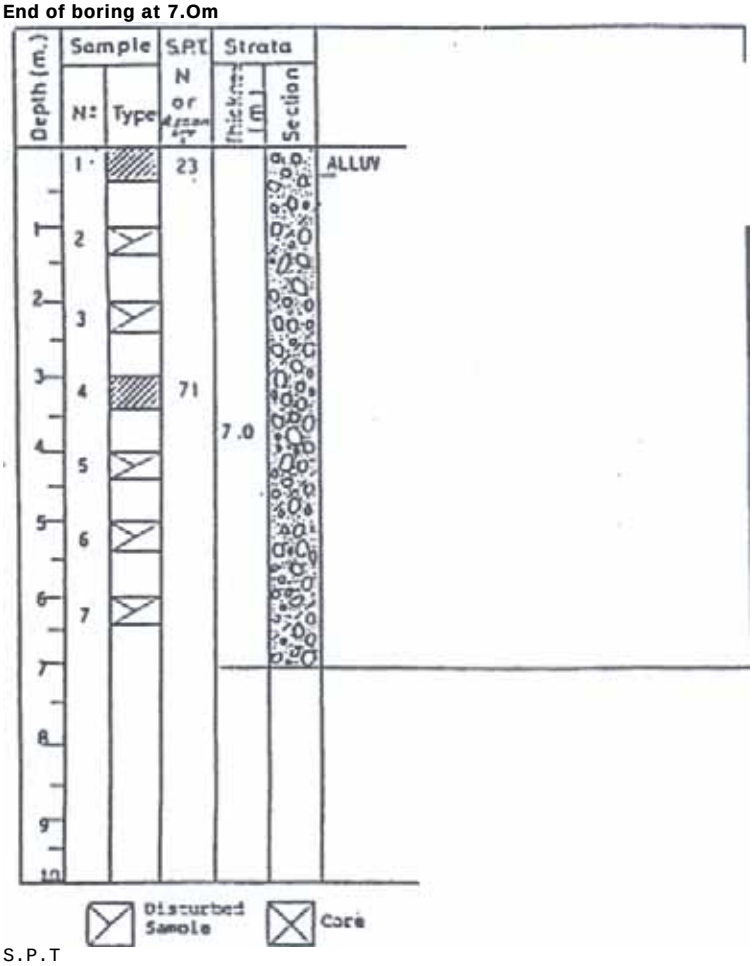

S.P.T

Fig. 2: **Lithologic log No.** BH2 **(from, Ardaman and Associates 1992)**

of soil profile development and surface weathering that characterize the older fans.

FIELD WORK FOR DATA ACQUISITION

Geoelectric resistivity field survey was carried out during November 1996, to collect the apparent resistivity data over a rectangular shaped area of about 30800 in z. The eastern side of the area (220 m long) is parallel to the coast of the Gulf of Suez. Horizontal electrical sounding (profiling method), using Wenner array, was chosen to perform this field work. Measurements were done at different electrode spacings (a). Since, by increasing the electrode spacing more of the injected current flows to greater depths and consequently apparent resistivity values at different depths are obtained. The electrode spacing varied from 1 m. up to 60 m. in order to cover the formations at different depths in **a comprehensive way.** So, **the field survey was completed at electrode spacings (a) equal 1, 5, 10, 15, 20, 30, SO and 60 meters and consequently the expected depths of penetration at these spacings would be 0.33, 1.65, 3.3, 4.95, 6.6, 9.9, 16.5 and 19.8 m., respectively (Roy and Apparao 1971). Table (1) contains the geometrical distribution of the collected data. These data were represented in isoapparent resistivity maps, as shown in Figs.** 3_a -10_a.

Table (1): The Geometrical Distribution of the Collected Horizontal Electrical Soundings (HES) . -

The electrode spacing (a) in meters	The distance between each two successive stations	The Number of HES over the area
1	10	13*21=273
5	10	13*21=273
10	20	7'`11=77
15	20	7* 11=77
20	40	4*6=24
30	40	4*6=24
50	40	4*6=24
60	40	4*6=24

DATA ANALYSIS:

Although the iso-apparent resistivity maps are often complex in their shapes, they can be interpreted mainly through a qualitative approach. Numerical smoothing techniques allow to define resistivity highs and lows and can enhance the qualitative interpretation of iso-apparent resistivity maps (Topfer 1976). The smoothing approaches are frequently applied in the interpretation of gravity and magnetic measurements, in order to separate the regional and residual components (Nettleton 1954).

In this paper, the least squares approach (Agocs 1951) was used for determining the best fitting regional to the observed data. The main advantage of this technique is its independent on grid spacing or on the systematic girding pattern (Topfer 1976). The best fitted data, that may be considered as a regional resistivity pattern, were removed to emphasize the local effects of sea water invasion on the shallow subsurface section.

This local resistivity anomaly will be represented by the residual component that resulted from the best fitting process. Therefore, the local resistivity component will be considered, in addition to the original iso-apparent resistivity maps. Accordingly, the iso-apparent resistivity maps will clarify the range and gradient.of resistivity contours over the area at different depths which they roughly show the general subsurface situation. Besides, the local resistivity contour maps will reflect the local variations in resistivity values and consequently represent the local subsurface geological influences. The local resistivity maps were reduced only to the zero contour in order to obtain the resistivity zoning maps. These local resistivity zoning maps will differentiate sharply between negative and positive zones. Negative resistivity zones are due to the invasion of sea water on the surface and shallow subsurface layers, while positive zones may be attributed to dry and/or compact sediments in the surface layers and to hard rocks in the subsurface.

DISCUSSION OF RESULTS

In this section, the iso-apparent resistivity contour maps, local resistivity contour maps and local resistivity zoning maps will be interpreted in terms of subsurface geologic inferences. From the general characteristics of these maps and based on the previous geologic and topographic information, these maps can be interpreted as follows:

Maps at a=1 m.

These maps (Figs. 3_a,) **represent the variations in the electrical resistivity values at an expected depth equals 0.33** m **(Apparao and Roy 1971). The iso-apparent resistivity map (Fig.** 3_a**) constructed at a=1 m shows a great variation in the apparent resistivity values of the surface soil layer. These values range from less than 10 Ohm.m to more than 380 Ohm.m. This wide resistivity range reflects a comparable wide variation in the soil constituents over the area.**

From the analysis of the local resistivity contour map (Fig. 3b), the positive residual resistivity closures can be attributed to dry and compact soils, while the negative closures are attributed to soil logging, seepage or to wet soils, taking the values of negative contour numbers in considerations. These (soil logging, seepage and soil wetting) are probably due to the rise of solutions by the capillary forces through the weakest paths. .

Most of the studied area is covered by negative resistivity values, which take a continuous path, as shown in Fig. (3j. **The degree of contamination with salts, as indicated by the negative contour values; increases with increasing distance from the sea (i.e. to the western direction). This is due to the increase of the concentration of the contaminants near the mountains in this surface layer.**

Maps at a=5 and 10 m.

These maps (Figs. 4a-c **and** S_a**J were constructed in order to gain information about the lateral variations in the apparent resistivity at expected depths to 1.65 and 3.3 m, respectively. The examination of the apparent resistivity contours (Figs.** 4_a and S_a) **reflects a general decrease in the ohmic values in comparison with the previous map**

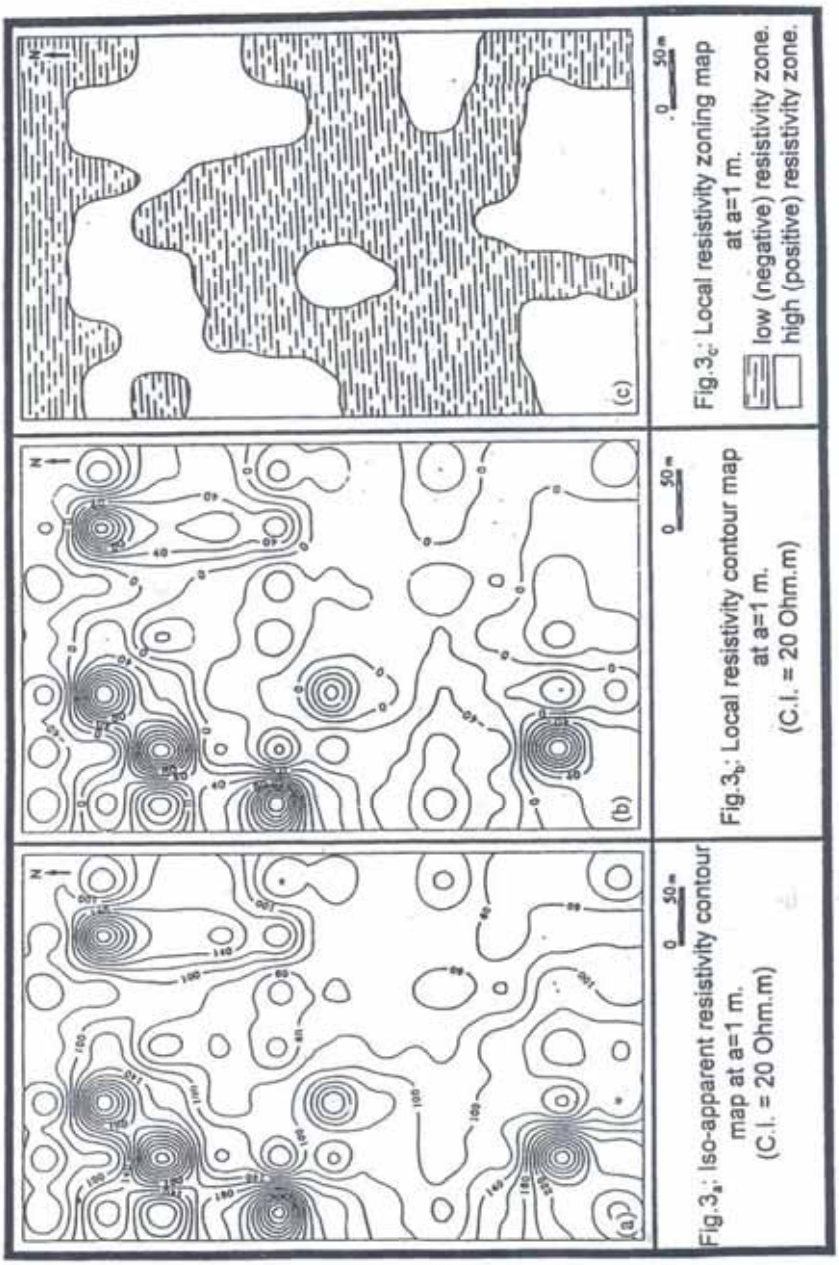

Fig.3$_a$: Iso-apparent resistivity contour map at a=1 m. (C.I. = 20 Ohm.m)

Fig.3$_b$: Local resistivity contour map at a=1 m. (C.I. = 20 Ohm.m)

Fig.3$_c$: Local resistivity zoning map at a=1 m.
low (negative) resistivity zone.
high (positive) resistivity zone.

(Fig. 3_a), since the resistivity range lies between $ and 223 Ohm.m. This is refereed to the increase of the soil moisture content and/or salinity. The most probable source of these effects is the capillary forces, since these two levels are topographically above the sea level. The solutions select high permeable paths with avoiding the compact zones in their uprising and this can be noticed from the local resistivity contour maps (Figs. 46 and Sb). These varying zones can be clearly distinguished on the local resistivity zoning maps (Figs. 4. and 5,

}.

Maps at a=15 *m.*

This iso-apparent resistivity map was constructed by contouring the apparent resistivity values measured at an electrode spacing (a) equals I S m (Fig. 6_a). This map, in addition to the calculated local resistivity contour and zoning maps (Figs. 66_J can reflect the lateral variations in the resistivity style at an expected depth of about 4.95 m.

The iso-apparent resistivity contours . show a continuous decrease in the measured resistivity values; attaining *a* resistivity range between 1.4 and 132 Ohm.m. These low ohmic values reflect the increase of water saturation in the porous media. The negative resistivity zone on the local resistivity contour and zoning maps appears as a discontinuous sheet. This discontinuous sheet is due to a horizontal invasion of sea water through porous paths.

Maps at a=20, *30 and 50 m.*

The apparent resistivity values collected at depths expected to be about 6.6, 9.9 and 16.5; m were used in constructing the iso-apparent resistivity maps shown in Figs. (7_a, 8_a and 9_a); respectively. A comparative examination of these maps shows a similarity in their patterns with a general decrease in their resistivity contour values with increasing the electrode spacing (a) and the depth of probing. Based on this examination and in the light of the geologic and topographic information it is expected that, the subsurface sediments are considered to be saturated with different percentages of water at these varying depths.

The inspection of the local resistivity contour and zoning maps of the three spacings (Figs. 7b_,;, $8b_c$ and 9b_J indicates the continuity of the negative resistivity zones through these levels to a large extent. This continuity can be attributed to the representation of the saturated porous materials at these levels. A clear positive resistivity zone can be noticed in the western side of the three zoning maps. This phenomenon can be attributed to mountainous prominence through the alluvial deposits. This positive zone diminishes in its size with increasing depth.

Maps at a=60 m.

The iso-apparent resistivity map (Fig. l 0_a) was constructed based on the resistivity values measured at a=60 m: It is clear from the analysis of this map that, there is a remarkable decrease in the resistivity contour values at an expected depth of about 19.8 m., since most of the contour numbers are less than 5 Ohm.m. The homogeneity of these low resistivity values is attributed to the increase of the concentrated salt water which acts as a highly conductive material in the pores filling solution.

From the inspection of the local resistivity contour map (Fig. l0b) it is noticeable that, the range of residual resistivity values over the area is reduced and lies between -

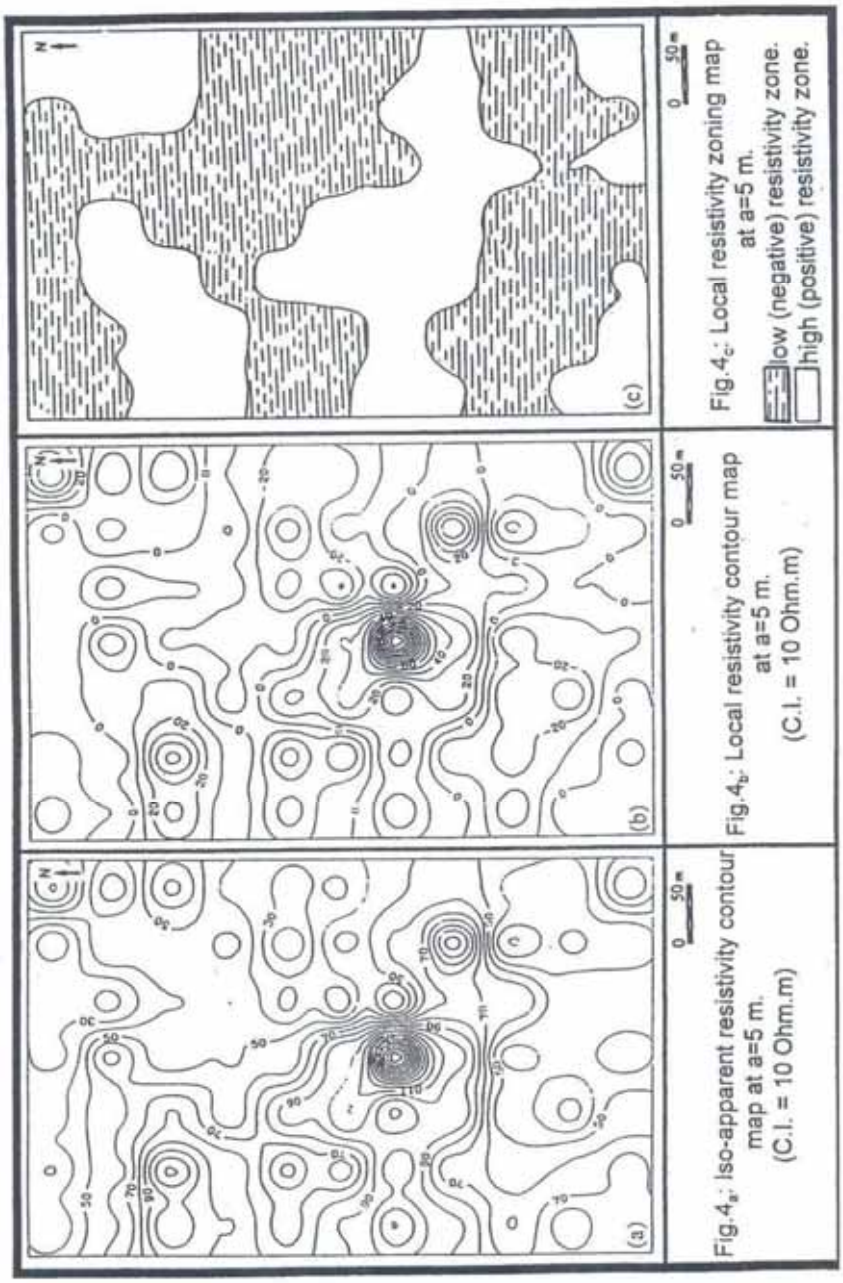

Fig.4$_a$: Iso-apparent resistivity contour map at a=5 m. (C.I. = 10 Ohm.m)

Fig.4$_b$: Local resistivity contour map at a=5 m. (C.I. = 10 Ohm.m)

Fig.4$_c$: Local resistivity zoning map at a=5 m.

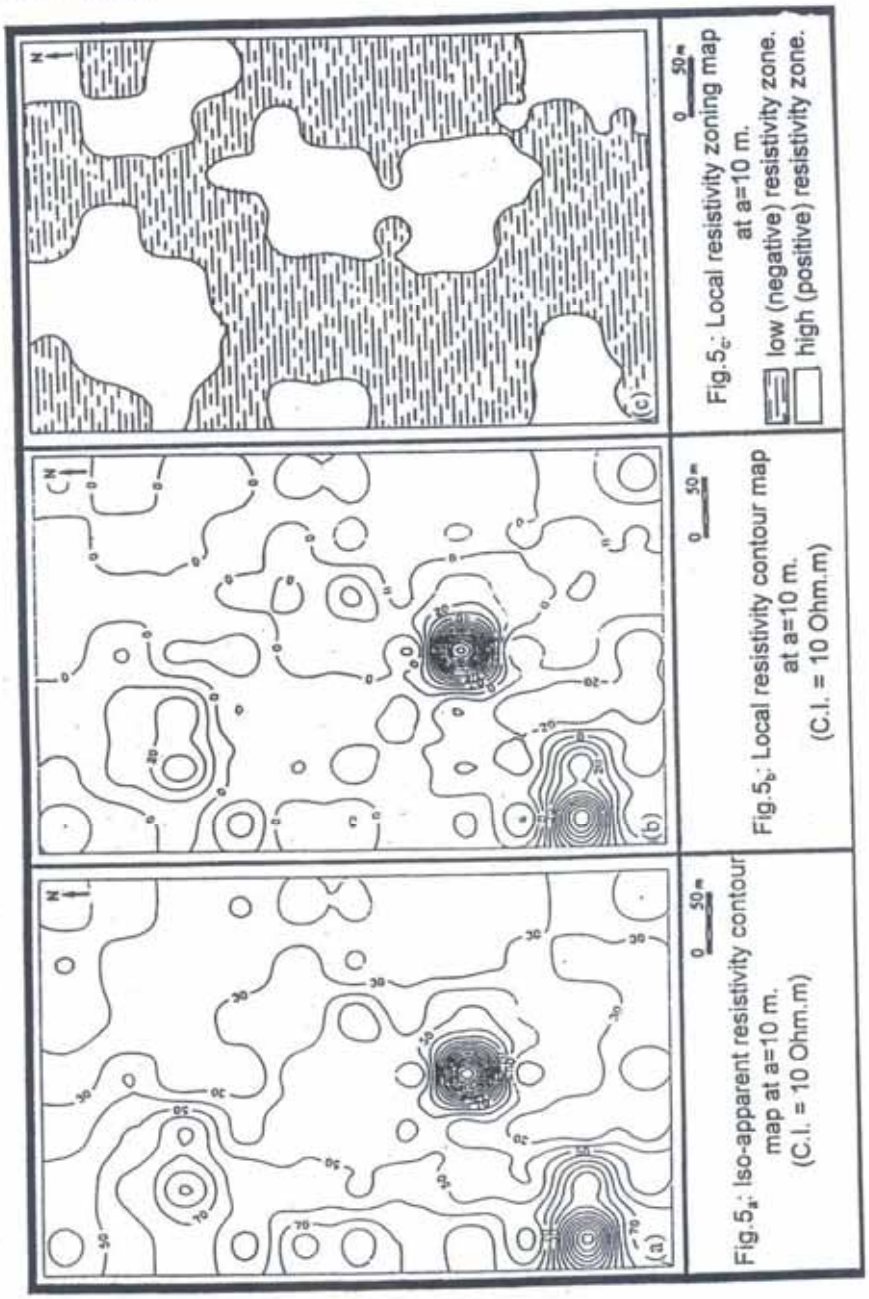

Fig.5$_a$: Iso-apparent resistivity contour map at a=10 m. (C.I. = 10 Ohm.m)

Fig.5$_b$: Local resistivity contour map at a=10 m. (C.I. = 10 Ohm.m)

Fig.5$_c$: Local resistivity zoning map at a=10 m.

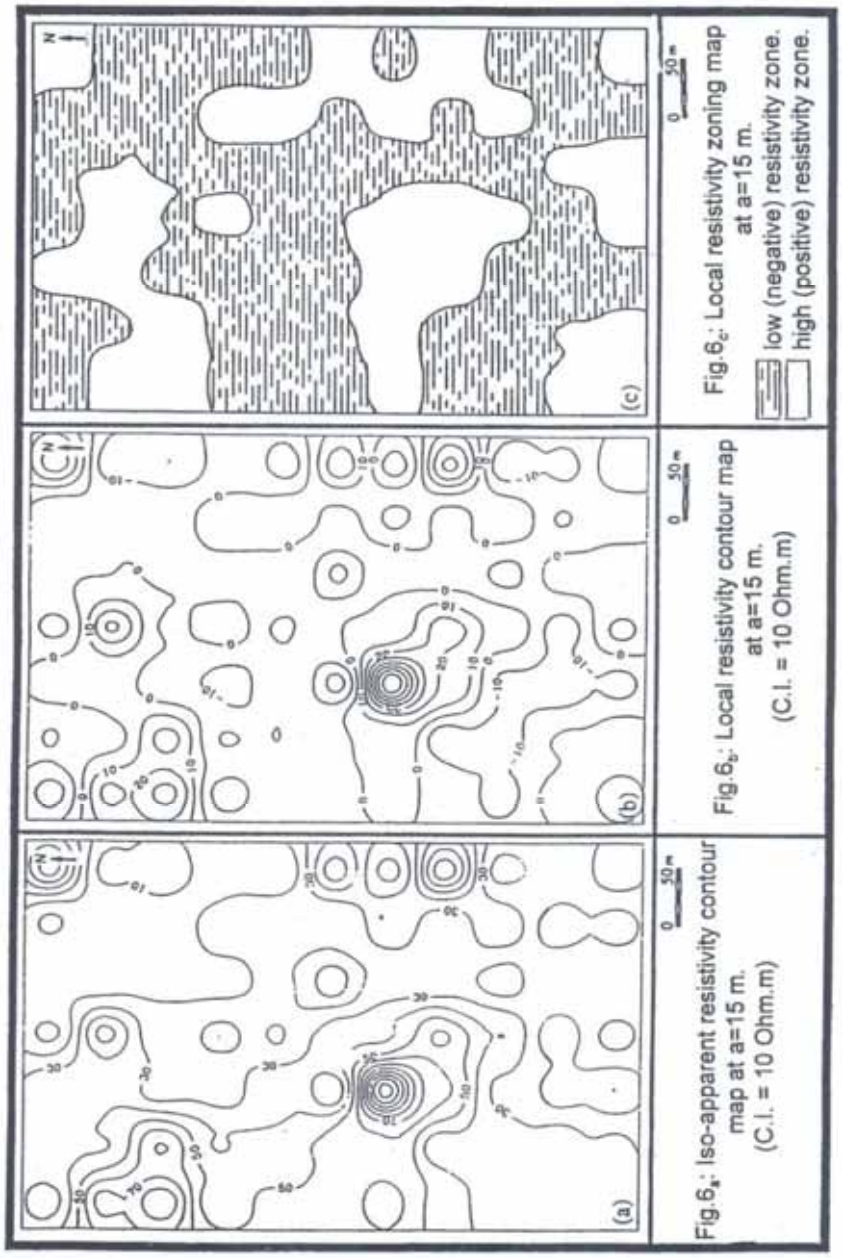

Fig.6$_a$: Iso-apparent resistivity contour map at a=15 m. (C.I. = 10 Ohm.m)

Fig.6$_b$: Local resistivity contour map at a=15 m. (C.I. = 10 Ohm.m)

Fig.6$_c$: Local resistivity zoning map at a=15 m.

2.6 and 3.8 Ohm.m. This very low resistivity spectrum indicates the increase of the conduction over the area at this depth. The local resistivity zoning map reflects the disappearance of the positive anomaly found in the western side of the previous three maps (Figs. 7, 8_c and 9_c). Therefore, the mountainous prominence body present at levels of the previous maps disappeared and consequently it is dangerous to select such sites for constructing heavy buildings.

CONCLUSIONS

A detailed geoelectric resistivity survey was executed using the horizontal electrical sounding approach with Wenner array. Eight iso-apparent resistivity contour maps were constructed at electrode spacings equal l, 5, 10, 15, 20, 30, 50 and 60 m.; in order to study the lateral variations in the geoelectric behavior at depths expected to be equal to 0.33, 1.65, 3.3, 4.95, 6.6, 9.9, 16.5 and 19.8 m; respectively.

The qualitative interpretation of these maps reflects that the measured apparent resistivity values decrease with increasing depths: This resistivity decrease is attributed to the increase of the conducting materials with depth.

The regional resistivity pattern was removed from the measured apparent resistivity data and the residual resistivity component is obtained using the least squares method; in order to accentuate the effects of sea water on the subsurface. Residual resistivity zoning maps were constructed by considering the zero contours to distinguish between the positive and negative zones. Negative resistivity zones are attributed to contaminated soils in the upper layers and to salt water intrusions with various degrees in the deeper layers. The degree of contamination was indicated by the value of negative contours. High (positive) resistivity zones wich occurred in the local contour and zoning maps were attributed to dry and compact materials in the soil layers and to hard rocks as mountainous prominence at deeper levels.

The integrated analysis of the iso-apparent resistivity contour maps, local resistivity contour maps and local resistivity zoning maps in the light of geologic and topographic information indicates:

1- The presence of inhomogeneous materials in the uppermost soil layer up to 0.33 m depth. These materials range from dry and compact to wet and salty sediments.
2- The porous media were partially saturated to different degrees at expected depths equal 1.65, 3.3 and 4.95 m. This saturation process was controlled by the capillary forces.
3- At depths equal to 6.6, 9.9, 16.5 and 19.8 m the porous media are considered to be saturated with sea water. This result is noticed by the general decrease of resistivity values. The rapid decrease in the local resistivity values with depth indicates the increase of the contaminated materials with increasing depth.
4- The subsurface destructive effects of sea water intrusions on the hard rocks was noticed and should be considered in the construction purposes.

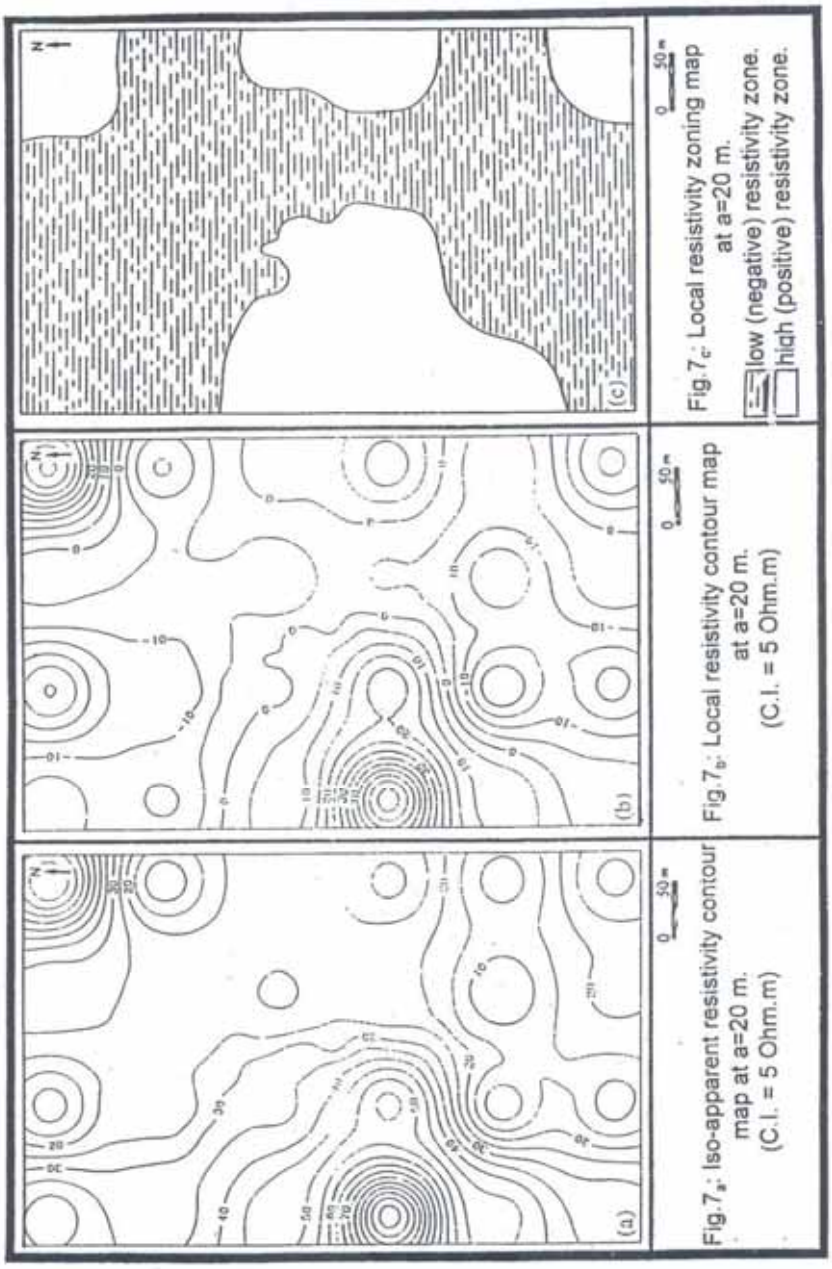

Fig.7$_a$: Iso-apparent resistivity contour map at a=20 m. (C.I. = 5 Ohm.m)

Fig.7$_b$: Local resistivity contour map at a=20 m. (C.I. = 5 Ohm.m)

Fig.7$_c$: Local resistivity zoning map at a=20 m.

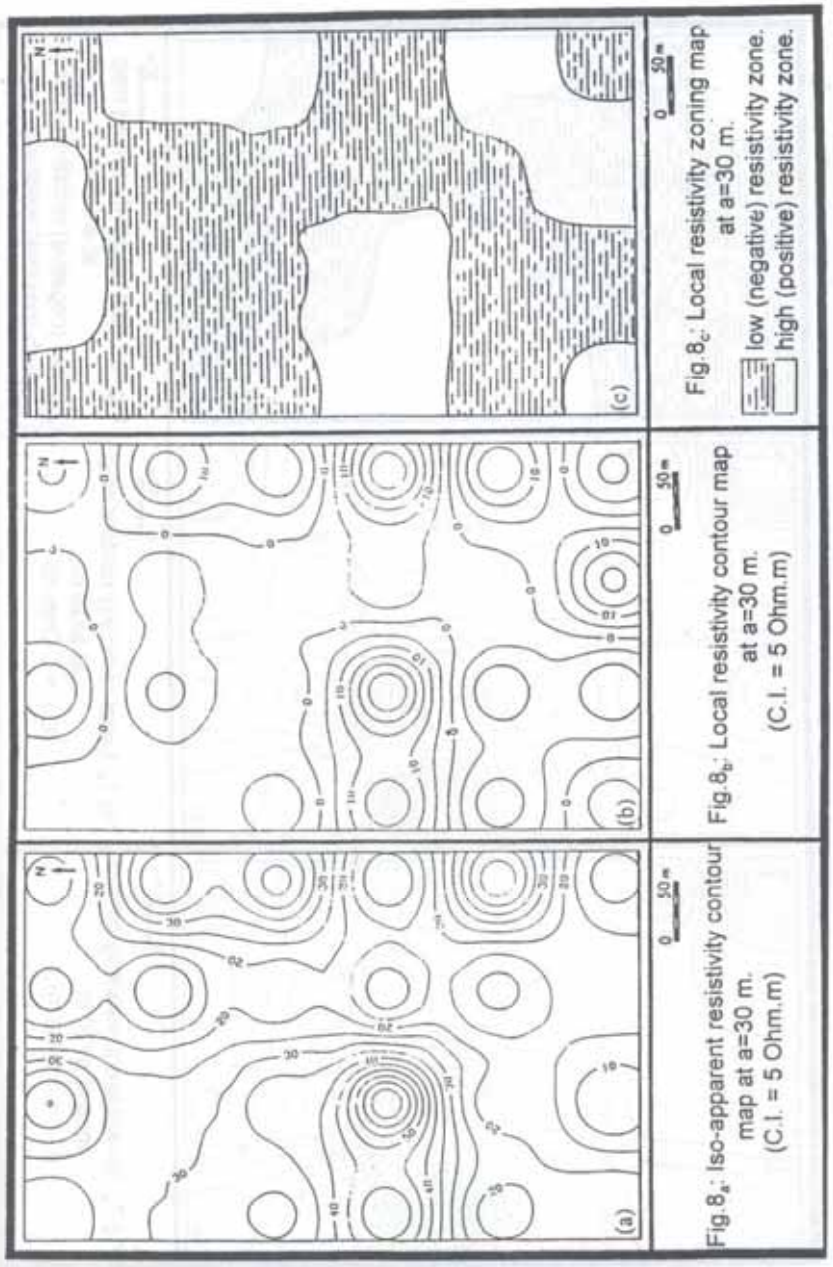

Fig.8$_a$: Iso-apparent resistivity contour map at a=30 m. (C.I. = 5 Ohm.m)

Fig.8$_b$: Local resistivity contour map at a=30 m. (C.I. = 5 Ohm.m)

Fig.8$_c$: Local resistivity zoning map at a=30 m.
low (negative) resistivity zone.
high (positive) resistivity zone.

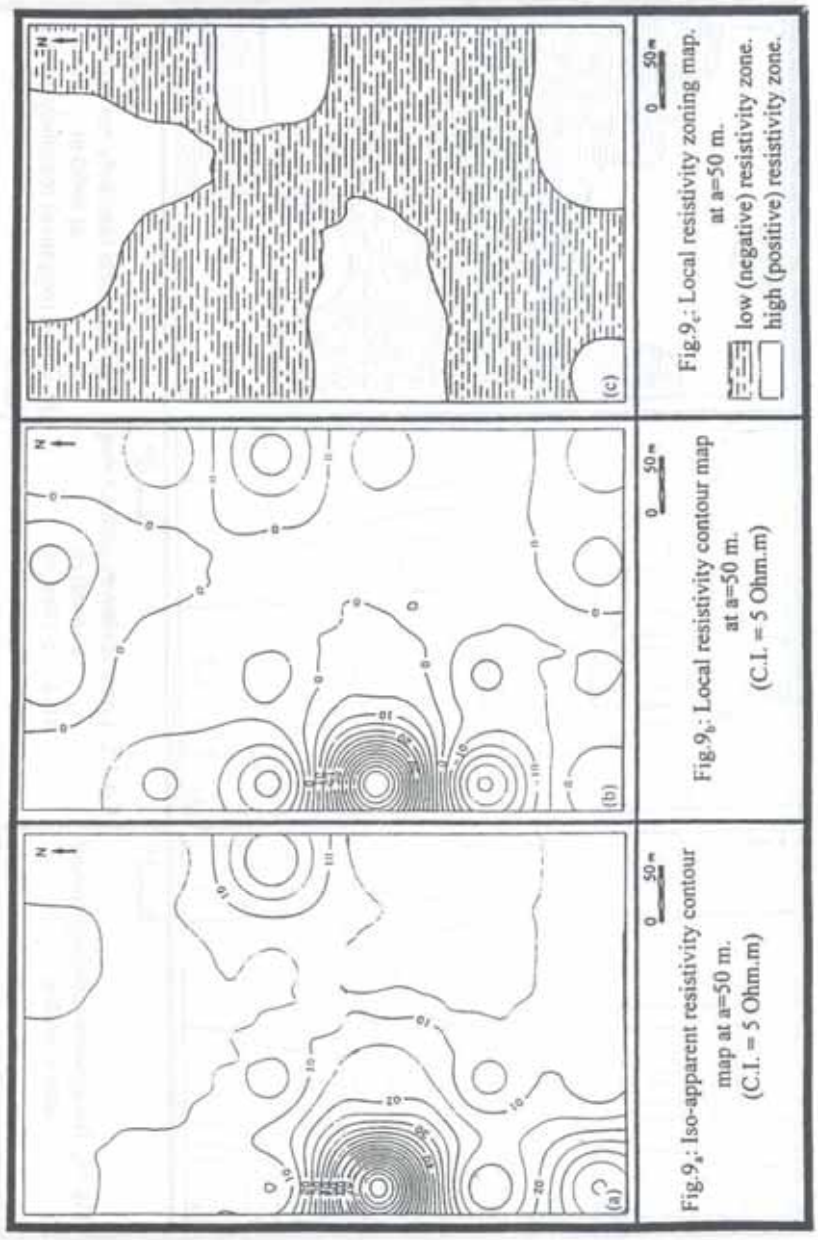

Fig.9$_a$: Iso-apparent resistivity contour map at a=50 m. (C.I. = 5 Ohm.m)

Fig.9$_b$: Local resistivity contour map at a=50 m. (C.I. = 5 Ohm.m)

Fig.9$_c$: Local resistivity zoning map. at a=50 m.
low (negative) resistivity zone.
high (positive) resistivity zone.

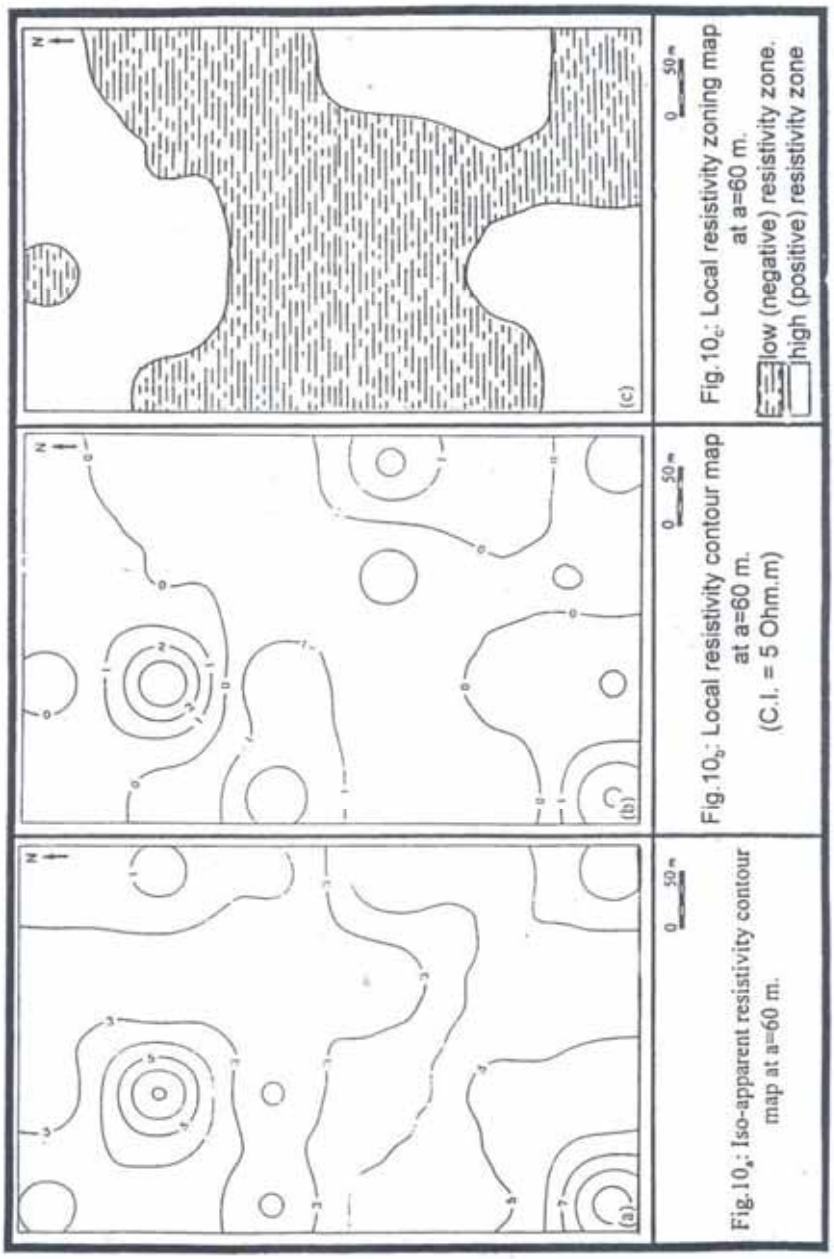

Fig.10$_a$: Iso-apparent resistivity contour map at a=60 m.

Fig.10$_b$: Local resistivity contour map at a=60 m. (C.I. = 5 Ohm.m)

Fig.10$_c$: Local resistivity zoning map at a=60 m.

Acknowledgment

I would like to express my deep thanks to the German Academic Exchange Service (DAAD) for the funding provided. Also, I am grateful to Prof. Dr. Berktoldhead of Geotechnical Environmental Geophysics Research Group, Institute of Geophysics, Munich , Germany- for his going through the manuscript and for his valuable discussions.

REFERENCES

Abdel-Fattah, Th.; El-Nekhaily, A.; El-Raey, M. A.; Abdel-Aziz, M. Z. and Morsi, M., 1988: Geoelectrical exploration for groundwater protection from sludge disposal on land near Alexandria city, Egypt. Proc. Of 1^{t} Symp. on Environ. Sciences, Inst. Of Grad. Stud. & Res. Alexandria University. pp. 102-122.

Agocs, W. B., 1951: Least-squares residual anomaly determination. Geophysics. V. 16: pp. 686-696.

Apparao, A. and Roy, A., 1971: Resistivity models experiments, 2. Geoexploration. V. 9., pp: 195-205.

Apparao, A., 1991: Geoelectric profiling. Geoexploration. V. 27, pp. 351-389.

Ardaman and Associates, Inc., 1992: Subsurface exploration, laboratory testing, conceptual design and construction recommendations. Canal Cities Water and Wastewater Phase II Project, City of Suez, Egypt. (unpublished technical reports).

Benson, A., K:, 1992: Integrating ground penetrating radar and electrical resistivity data to delineate groundwater contamination. Proceedings of the 4$^{`h}$ Int. Con. On G.P.R., June 8-13, Finland, Special Paper. V. 16; pp. 197-203.

Benson, A. K., Payne, K. L. and Stubben, M. A., 1997: Mapping groundwater contamination using D.C. resistivity and VLF geophysical methods - A case study. Geophysics. V. 62, pp. 80-86.

Bhattacharya , B. B.; Jain, S. C. and Mallick, K., 1974: Geophysical prospecting for barite. Geophys. Prosp. V. 22, pp.421-429.

Burger, H. R., 1992: Exploration geophysics of the shallow subsurface. Prentice-Hill, Inc.

Bush, P.; Cooke, R. U.; Burunsden, D.; Doornkamp, J. C. and Jones, D. K. C.; 1980: Geology and geomorphology of the Suez city region, Egypt. Journal of Arid Environments V. 3, pp. 265-281.

El-Hefnawy, M. A.; Abdallah, K; and Aboul-Fotouh, M. A.; 1984: Geo-electrical study on the groundwater in the western part of fVadi Badaa, Eastern Desert, Egypt. E.G.S. Proc. Of 3^{r-d} Ann. Meet., pp.285-31 1.

Flathe, H., 1954: Possibilities and limitations in applying geoelectrical methods to hydrogeological problems in the coastal areas of North West Germany. Geophys. Prosp. V. 3, pp. 95-110.

Keller, G. and Frischknecht, F. 1966: Electrical methods in geophysical prospecting. Pergamon Press, New York. 517 p.

Kelly, W. E., 1976: Geoelectric sounding for delineating groundwater contamination. Ground Water; V. 14, pp. b-10

Lanz; E.; Jemmi, L.; Muller, R.; Green, G.; Pugin, A; and Huggenberger, P.; 1994: Integrated studies of Swiss waste disposal sites: results from georadar and other geophysical surveys. Proceedings of the 5`h Int. Con. On G.P.R., June 12-16, Kitchener, Ontrio, Canda., pp. 1261-1274.

Mazac, O.; Kelly, W. E.; and Landa, L; 1987: Surface geoelectric for groundwater pollution and protection studies. Journal of Hydrol., V. 93, pp. 277-294. -

Nettleton, L. L., 1954: Regionals, residuals and structures. Geophysics. V. 19, pp. 1-22.

Said, R., 1962: The geology of Egypt. Elsevier Publ. Co., Amsterdam, New York. 337p.

Shendi, E. H., 1995: Regional-residual resistivity anomalies as an effective indicator for ground water salinity. E.G.S . Proc. Of the 13`h Ann. Meet., pp. 351-364.

Telford; W. H., Gilbert, L. P. and Sherif, R. E., 1990: Applied geophysics. 2"d Edition, Cambridge University Press., London 770 p.

Topfer, K.D., 1976: Representation and interpretation of resistivity mapping data in groundwater prospecting in Zambia. J. Geophys. V. 42, pp. 147-158.

Zohdy, A.; Eaton, G. and Mabey, D. 1974: Application of surface geophysics to ground water investigations. U.S.G.S., Book 2, Chapter D.